

# UCLA

## UCLA Previously Published Works

### Title

Assessing the aneurysm occlusion efficacy of a shear-thinning biomaterial in a 3D-printed model

### Permalink

<https://escholarship.org/uc/item/4cp1v15b>

### Authors

Schroeder, Grant  
Edalati, Masoud  
Tom, Gregory  
[et al.](#)

### Publication Date

2022-06-01

### DOI

10.1016/j.jmbbm.2022.105156

Peer reviewed



Published in final edited form as:

*J Mech Behav Biomed Mater.* 2022 June ; 130: 105156. doi:10.1016/j.jmbbm.2022.105156.

## Assessing the aneurysm occlusion efficacy of a shear-thinning biomaterial in a 3D-printed model

Grant Schroeder<sup>a,b,c</sup>, Masoud Edalati<sup>a,b,d</sup>, Gregory Tom<sup>a,b</sup>, Nicole Kuntjoro<sup>a,b</sup>, Mark Gutin<sup>a,b,e,f</sup>, Melvin Gurian<sup>e,f</sup>, Edoardo Cuniberto<sup>e,f</sup>, Elisabeth Hirth<sup>e,f</sup>, Alessia Martiri<sup>e,f</sup>, Maria Teresa Sposato<sup>e,f</sup>, Selda Aminzadeh<sup>a,b</sup>, James Eichenbaum<sup>a,b</sup>, Parvin Alizadeh<sup>a,b,g</sup>, Avijit Baidya<sup>a,b</sup>, Reihaneh Haghniaz<sup>a,b,h</sup>, Rohollah Nasiri<sup>a,b</sup>, Naoki Kaneko<sup>i</sup>, Abraham Mansouri<sup>j</sup>, Ali Khademhosseini<sup>a,b,h,\*</sup>, Amir Sheikhi<sup>a,b,k,l,\*</sup>

<sup>a</sup>Department of Bioengineering, University of California, Los Angeles, 410 Westwood Plaza, Los Angeles, CA 90095, USA

<sup>b</sup>California NanoSystems Institute (CNSI), University of California, Los Angeles, 570 Westwood Plaza, Los Angeles, CA 90095, USA

<sup>c</sup>David Geffen School of Medicine at UCLA, Los Angeles, California, USA

<sup>d</sup>Department of Mechanical Engineering Rowan University, Rowan Hall 201 Mullica Hill Rd. Glassboro, NJ 08028, USA

<sup>e</sup>Biomaterials Innovation Research Center, Division of Biomedical Engineering, Department of Medicine, Brigham and Women's Hospital, Harvard Medical School, Cambridge, MA 02139, USA

<sup>f</sup>Harvard-MIT Division of Health Sciences and Technology, Massachusetts Institute of Technology, Cambridge, MA 02139, USA

<sup>g</sup>Department of Materials Science & Engineering, Faculty of Engineering & Technology, Tarbiat Modares University, Tehran, Iran

<sup>h</sup>Terasaki Institute for Biomedical Innovation (TIBI), Los Angeles, CA 90024, USA

<sup>i</sup>Department of Radiological Sciences, David Geffen School of Medicine, University of California, Los Angeles, 10833 Le Conte Ave, Los Angeles, CA 90095, USA.

<sup>j</sup>Department of Mechanical Engineering, Higher College of Technology, Dubai, 15825, UAE

\*Corresponding authors: Prof. A. Khademhosseini, khademh@terasaki.org; Prof. A. Sheikhi, sheikhi@psu.edu.

**Publisher's Disclaimer:** This is a PDF file of an unedited manuscript that has been accepted for publication. As a service to our customers we are providing this early version of the manuscript. The manuscript will undergo copyediting, typesetting, and review of the resulting proof before it is published in its final form. Please note that during the production process errors may be discovered which could affect the content, and all legal disclaimers that apply to the journal pertain.

### Conflict of Interest

A. K. is a co-founder of a start-up company, Obsidio, Inc., which is based on shear-thinning embolic materials.

### Declaration of interests

The authors declare that they have no known competing financial interests or personal relationships that could have appeared to influence the work reported in this paper.

Ali Khademhosseini reports financial support was provided by National Institutes of Health. Ali Khademhosseini reports a relationship with Obsidio, Inc that includes: board membership and equity or stocks. Ali Khademhosseini has patent Shear-thinning compositions as an intravascular embolic agent issued to Obsidio, Inc.

<sup>k</sup>Department of Chemical Engineering, The Pennsylvania State University, University Park, PA 16802, USA

<sup>l</sup>Department of Biomedical Engineering, The Pennsylvania State University, University Park, PA 16802, USA

## Abstract

Metallic coil embolization is a common method for the endovascular treatment of visceral artery aneurysms (VAA) and visceral artery pseudoaneurysms (VAPA); however, this treatment is suboptimal due to the high cost of coils, incomplete volume occlusion, poor reendothelialization, aneurysm puncture, and coil migration. Several alternative treatment strategies are available, including stent flow diverters, glue embolics, gelfoam slurries, and vascular mesh plugs—each of which have their own disadvantages. Here, we investigated the *in vitro* capability of a shear-thinning biomaterial (STB), a nanocomposite hydrogel composed of gelatin and silicate nanoplatelets, for the minimally-invasive occlusion of simple necked aneurysm models. We demonstrated the injectability of STB through various clinical catheters, engineered an *in vitro* testing apparatus to independently manipulate aneurysm neck diameter, fluid flow rate, and flow waveform, and tested the stability of STB within the models under various conditions. Our experiments show that STB is able to withstand at least 1.89 Pa of wall shear stress, as estimated by computational fluid dynamics. STB is also able to withstand up to 10 mL s<sup>-1</sup> pulsatile flow with a waveform mimicking blood flow in the human femoral artery and tolerate greater pressure changes than those in the human aorta. We ultimately found that our *in vitro* system was limited by supraphysiologic pressure changes caused by aneurysm models with low compliance.

## Keywords

shear-thinning biomaterials; visceral artery aneurysms; pseudoaneurysms; silicate nanoplatelets; minimally invasive; hydrogels; catheters

## 1. Introduction

Visceral artery aneurysms (VAA) and visceral artery pseudoaneurysms (VAPA) are rare, but deadly vascular malformations that can present in an emergency setting as an acute rupture or as an incidental finding on medical imaging.<sup>1,2</sup> Of the VAA found incidentally on imaging, 10–20% will proceed to rupture, resulting in a 20–70% mortality rate, depending on the aneurysm location and availability of treatment.<sup>3</sup> The treatment of a VAA that has either ruptured or is at a high risk of rupturing involves either surgical repair or endovascular treatment.<sup>1</sup> Endovascular treatment has emerged as the preferred method, since its mortality is only 2.7% compared to 23.9% with surgical treatment,<sup>4</sup> can be more widely utilized in patients with comorbidities, and is associated with reduced lengths of hospital stays.<sup>5</sup>

Endovascular placement of metallic coils into VAA and VAPA is the current mainstay of treatment;<sup>6,7</sup> however, metallic coils are associated with less than 50% occlusion of the aneurysm sac,<sup>8</sup> poor reendothelialization of the aneurysm orifice,<sup>9</sup> coil migration into adjacent structures,<sup>10,11</sup> recanalization/aneurysm recurrence,<sup>12</sup> and high cost.<sup>13</sup> They are also poorly suited for occlusion of VAPA, which commonly have narrow necks and have

a 76.3% risk of rupture,<sup>14</sup> because complete parent vessel occlusion is usually required to avoid complications such as coil migration into adjacent viscera.<sup>7,15</sup> Current alternatives to coils include stent flow diverters, which can be limited by surrounding vessel architecture and are highly expensive, glue embolics, which may be associated with a high degree of reflux and non-target embolization as well as catheter entrapment, gelfoam slurries, which are only temporary embolizing agents, and vascular mesh plugs, which are more expensive than coils and sacrifice distal blood flow.<sup>7</sup> Onyx is another liquid embolic agent that forms a solid upon release from a catheter and has been used in the treatment of aneurysms;<sup>16</sup> however, it has been associated with cases of catheter entrapment within the solidified material<sup>17</sup> and contains dimethyl sulfoxide (DMSO), which is associated with angiotoxicity.<sup>18</sup>

Since no alternative agent has displaced metallic coils as the mainstay of aneurysm occlusion to date, we considered the potential of STB, a nanocomposite hydrogel composed of gelatin and silicate nanoplatelets, for aneurysm occlusion. STB has previously been shown to be successful in similar applications including superficial hemostasis promotion<sup>19</sup> and complete endovascular embolization of large blood vessels for hemorrhage treatment.<sup>20</sup> Potential advantages to STB include its non-adhesiveness, cost-effective production, and lack of DMSO. In this study, we seek to answer the question of whether STB can successfully occlude *in vitro* aneurysm models under varying shear stress. To accomplish this goal, we fabricate 3D-printed aneurysm models, connected to a physiological flow pump similar to prior systems,<sup>21–23</sup> and manipulate flow rates and waveform patterns to test the STB stability. We hypothesize that STB will be stable under physiologically relevant flow conditions, but increasing shear stress on the STB within the aneurysm models will eventually cause STB failure, since prior studies have determined high wall shear stress as an initiator of aneurysm formation,<sup>24</sup> as well as a driver of recanalization of aneurysms occluded by metallic coils and Onyx liquid embolic agent.<sup>25</sup> The outcome of this study may provide insights for designing stable STB for minimally invasive aneurysm occlusion.

## 2. Materials and methods

### 2.1. STB formulation

STB was formulated according to a method we previously described.<sup>19</sup> Briefly, a stock solution (18% w/v) of gelatin type A derived from porcine skin (Sigma-Aldrich, MO, USA) in Milli-Q water (40 °C), as well as a stock solution (9% w/v) of LAPONITE® XLG-XR synthetic silicate nanoplatelets (Southern Clay Products, Inc. Louisville, KY) in cold Milli-Q water (4 °C) were prepared. The nanoplatelet gel was then allowed to warm to room temperature before portions of the stock solutions were mixed together with the addition of extra Milli-Q water to yield the final 6% w/v nanocomposite with 75% of the weight being silicate nanoplatelets. The constituents were then mixed via 5 rounds of vortexing at 3000 rpm for 5 min, followed by manual mixing with a spatula for 2 min. The STB was then stored at 4 °C until use.

## 2.2. Injection force of STB

The force required to vertically depress a syringe plunger and move STB through catheters was measured using an Instron mechanical tester (model 5943, MA, USA). STB was loaded into either a 3 mL or 1 mL syringe (BD Biosciences, CA, USA, internal diameters of 8.66 and 4.78 mm, respectively), connected to a catheter via a Luer lock mechanism, and secured to the Instron mechanical tester using a tensile grip at the bottom. The upper compressive plate of Instron was depressed at a constant rate of  $33.96 \text{ mm min}^{-1}$ , which allowed for an STB injection rate of  $2.0 \text{ mL min}^{-1}$  through a 3 mL syringe connected to various sizes of catheters. These catheters were each 100 cm in length and included 4 F, 5 F, and 6 F sizes. An additional 3.1 F microcatheter of length 150 cm was tested in connection with a 1 mL BD syringe. An injection force plateau between 25 and 30 N for STB injected through a 3 mL BD syringe connected to a 4 F catheter was used as a quality-control measure to ensure that the STB quality was similar to our previous reports.<sup>20</sup> The same constant rate of depression was used for both 3 mL and 1 mL BD syringes. The injection force was recorded as the force of depression at 6 s of constant depression. The force required for injection was measured using a 100 N load cell and recorded using the Bluehill software (Bluehill3, Danderyd, Sweden).

## 2.3. Fabrication of 3D-printed *in vitro* aneurysm models

The *in vitro* aneurysm models were designed in two parts, top and bottom halves, allowing for facile dismantling. The top half comprised a hemisphere of the assigned aneurysm sac (diameter 1 cm or 3 cm). The bottom part consisted of the bottom hemisphere sac, connected by a 5 mm long neck of variable diameters (2 mm to 6 mm) to a cylindrical blood vessel with a diameter of 6 mm and a length of 75 mm. To accomplish this, we first developed a computer-aided design (CAD) model of desired aneurysm sizes and parent artery (Figure 1A). Components were fabricated by 3D printing the hemispheres and blood vessels with the necks using acrylonitrile butadiene styrene (ABS) filament (Lulzbot, ND, USA) (Figure 1B), before being polished (Figure 1C). These pieces were glued into custom-built laser-cut (Wavelength Laser Services, Inc., MA, USA) acrylic boxes that were then filled with polydimethylsiloxane (PDMS) (Ellsworth Adhesives, CA, USA) at a 10:1 base-to-crosslinker ratio and cured in the oven for 1 h at  $80^\circ\text{C}$ . The PDMS was removed from the molds, and the remaining ABS was dissolved from the PDMS casting using acetone (purity  $> 99\%$ , Fisher Scientific, PA, USA) (Figure 1D). The completed models were assembled between two acrylic plates bolted together to compress the two pieces of aneurysm model during flow experiments (Figure 1E).

Regarding model dimensions, we fabricated saccular aneurysm models with varying neck diameters ranging from 2 mm to 6 mm, and a sac diameter of either 1 cm or 3 cm. These most resemble VAPA, which tend to have narrower necks. The diameters of the spherical aneurysm models were chosen to reflect the size of typical small and large aneurysms that are commonly treated clinically.<sup>23</sup> The 3 cm models were used to assess the feasibility and time of injecting large volumes of STB into large aneurysm sacs, since larger aneurysms inherently take longer to fill. The 1 cm models used for 24 h pulsatile flow experiments for STB largely for material conservation—since the STB-fluid interface was the primary area of interest in these experiments, and it is the same area for both the 3 cm and 1 cm models.

Other relevant dimensions in our aneurysm models include a neck length of 5 mm and a parent blood vessel diameter of 6 mm. A neck length of 5 mm enabled us to better visualize the material loss before being carried away by the main underlying vessel, which helped determine the mechanism of STB loss. The diameter of parent blood vessel was selected to be 6 mm since this was the average diameter of the most common celiac trunk branches to be affected by VAA: splenic artery = 5.3 mm, common hepatic artery = 5.0 mm, celiac trunk = 7.9 mm.<sup>24</sup> In reality, the shapes of VAA and VAPA are highly variable, and we recognize that it is not practical to create models for every subtype of aneurysm shape and that some features of our design decrease stresses placed on the STB in the aneurysm sac. For example, we used a straight parent blood vessel in our models, and it is known that increased parent vessel curvature increases aneurysm inflow volume rates and velocities.<sup>25</sup> Additionally, the aneurysm neck was oriented perpendicularly to the parent blood vessel, which decreases the normal stress of fluid flow toward the aneurysm compared to if the aneurysm were located at the origin of a bifurcation.<sup>26</sup> These effects decrease fluid flow into the aneurysm sac, which is associated with a higher likelihood of successful aneurysm occlusion/thrombosis.<sup>27</sup> We also recognize that saccular aneurysms tend to form at blood vessel bifurcations and curvatures that lead to abnormal wall shear stress,<sup>28</sup> and that splenic artery aneurysms—the most common form of VAA—tend to form along more tortuous vessels.<sup>29</sup> Knowing that our fabrication method could be easily manipulated to produce patient-specific aneurysm models in the future, and that we could increase shear stress by increasing flow rates and aneurysm neck widths, we chose to construct basic symmetrical models that allowed for consistent STB loading and recovery for the purpose of this study.

#### 2.4. Aneurysm model filling with a catheter

As a proof-of-concept demonstration of the feasibility of filling an *in vitro* aneurysm model with a catheter, we navigated a 100 cm long 5 F catheter into a 3 cm aneurysm model experiencing a pulsatile flow of Dulbecco's phosphate buffered saline (DPBS) (Fisher Scientific, Hampton, NH) at  $10 \text{ mL s}^{-1}$  that mimics the flow waveform of the human femoral artery. Then, STB was injected through the catheter by hand and filled the aneurysm model in less than 1 min (Figure 1F and Supplemental Video 1). Images were taken to demonstrate the stability of the material and the required time to fill the large aneurysm.

#### 2.5. In vitro flow experiments (3 min visualizations and 24 h mass recovery)

For *in vitro* flow experiments, each model (2 mm to 6 mm neck diameters) was opened and both hemispheres were filled completely with STB with either a spatula or a syringe. The two hemispheres were then placed together between acrylic plates that were bolted together to compress the two PDMS pieces. Each model was then linked to other models in series via plastic tubing (inner diameter of 6 mm, length of 50 mm) and connected to an AccuFlow-Q physiological flow pump system (Shelley Medical Imaging Technologies, Toronto, Canada). The pump, after being filled with DPBS, was turned on to generate either a constant flow or a pulsatile flow (AccuFlow-Q femoral artery setting) of the chosen flow rate ( $\text{mL s}^{-1}$ ). Each experiment was repeated at least 3 times. For 3 min visualization experiments, the stability of the STB within each aneurysm model was observed to evaluate the material loss. If even a small amount of STB exited the aneurysm sac, this was deemed an experimental failure. For the 24 h mass recovery experiments, the PDMS aneurysm models were weighed before

and after being loaded with the STB to determine the exact mass of STB left over. The flow was stopped after 24 h, and the aneurysm models were opened. A spatula was used to collect the remaining STB in the aneurysm sac and transfer it to a pre-weighed Eppendorf tube. The material was deep frozen for 24 h at  $-80\text{ }^{\circ}\text{C}$  and then freeze-dried (Labconco, MO, USA) for 48 h to remove any fluid from the dry STB mass. Additionally, a control sample of STB not exposed to the fluid flow was weighed before and after freeze-drying to determine the exact percent mass in each STB batch, which was approximately 6%. The precise STB dry mass percent for each batch was used to compare against the STB recovered from the models and calculate the percent remaining after 24 h.

## 2.6. Blood mimicking fluid (BMF) flow experiment

BMF (Shelley Medical Imaging Technologies, Toronto, Canada) was used to fill the AccuFlow-Q pump. This was done to visually assess how an increase in fluid viscosity of the BMF ( $4.1 \pm 0.1\text{ mPa s}$ ) may change the visual stability of STB at different conditions. The experimental setup was the same as the 24-h mass recovery experiments except that the mass recovered was not measurable because the BMF could not be removed from the STB.

## 2.7. Computational fluid dynamics (CFD) simulation

Three-dimensional finite element simulations were conducted using COMSOL Multiphysics® version 5.5 to model the flow in arterial geometries with an aneurysm filled with STB. Parameters such as the aneurysm size, flow rate, flow pattern, and neck diameter were explored. The computational domain is a finite length 3D conduit that is 100 mm long with an inner diameter of 6 mm, connected to an aneurysm sac through a 5 mm long cylindrical neck. To mimic the *in vitro* experimental protocol, the neck (i.e., STB-fluid interface) was capped. Both steady-state and time-varying flow (pulsatile flow) were considered at the flow rates of 10 to 15  $\text{mL s}^{-1}$ . Reynolds-averaged Navier-Stokes equations were solved over the 3D computational domain, and turbulent closure was achieved by using  $k-\omega$  turbulence model.<sup>30</sup> The Reynolds number in these studies varied between 3600 and 6000. The computational domain was divided into approximately 540,000 tetrahedral, prism, or triangular mesh elements, and near-wall condition was treated with the wall function. Inlet and outlet boundary conditions were applied at the computational domain with the no-slip condition at the wall. The maximum shear stress values due to both dynamic and turbulent viscosity were estimated at the STB-fluid cross-section inside the parent artery.

## 2.8. In vitro pressure measurement in aneurysm model

The pressure was measured within the *in vitro* system using a wireless pressure sensor (PASCO Scientific, CA, USA) and SPARKvue software version 4.0.0.18. The pressure sensor was connected to the *in vitro* system via a 3-way valve such that pressure changes within the system were detected by the sensor without disrupting forward fluid flow.

## 2.9. Statistical analysis

All statistical analyses and graphing were performed using GraphPad Prism (Version 8) software. One-way analysis of variance (ANOVA) with multiple comparisons using Fisher's least significant difference post-test was performed for data groups when comparing the

means of two groups (example: percent remaining of  $10 \text{ mL s}^{-1}$  pulsatile flow in 6 mm model versus  $15 \text{ mL s}^{-1}$  pulsatile flow in 6 mm model). One-way ANOVA with multiple comparisons using the Tukey post-test was performed for data groups when comparing the means of all groups (example: percent remaining for each flow pattern compared to other flow patterns). Statistically significant differences were defined as  $P < 0.05$ . Asterisks and corresponding P values were defined as the following: \* =  $P < 0.05$ , \*\* =  $P < 0.01$ , \*\*\* =  $P < 0.001$ , \*\*\*\* =  $P < 0.0001$ .

### 3. Results and discussion

#### 3.1. STB formulation, properties, and injectability

We first prepared a stable and injectable STB, comprising silicate nanoplatelets and gelatin (Figure 2A). The STB formulation is 6% w/v nanocomposite with 75% of it being silicate nanoplatelets for our investigation. We previously found that this STB has desirable viscoelastic properties while remaining injectable through catheters due to its ability to flow under high shear rates.<sup>19,20,31</sup> Through clinically relevant catheters, STB was injectable and formed a self-sustaining structure upon injection (Figure 2B). To ensure the consistency of STB fabrication, we measured the force required to inject the STB through a range of clinical catheters (100 cm long, 4–6 F) attached to a 3 mL syringe at a constant rate ( $33.96 \text{ mm min}^{-1}$ ) of syringe depression (Figure 2C). The injection force plateaus did not fluctuate, attesting to a homogenous STB, and their values depended on the catheter diameter: the larger the catheter diameter, the smaller the injection force plateau value. As an example, the injection force via the 5 F catheter was between 25 N and 30 N, being consistent with our prior reports using the same injection parameters.<sup>20</sup> The effect of clinical catheter gauges on the STB injection force plateaus for 3 mL and 1 mL syringes are shown in Figures 2D and 2E, respectively. Given the relationship of force equaling the product of area and pressure, the STB demonstrated a substantial reduction in force required for injection using a 1 mL syringe with a smaller internal diameter compared with the 3 mL syringe (4.78 mm versus 8.66 mm, respectively). Of note, an additional 3.1 F microcatheter of length 150 cm was tested in connection with the 1 mL BD syringe.

#### 3.2. In vitro flow experiments

After confirming the STB injectability into the *in vitro* models as shown in Figure 1F, the stability of STB under physiological pulsatile flow was assessed using an *in vitro* experimental setup shown in Figure 3. Using 1 cm diameter aneurysm models with neck widths ranging from 2 mm to 6 mm (Figure 3A), the models were connected to a pump in series, as shown in Figures 3B and 3C, with STB filling each aneurysm sac (Figure 3D). Relatively narrow necks were selected to model VAA and VAPA that are most suitable for coil embolization.<sup>32</sup> First, maximum flow rates tolerated by the STB for at least 3 min were determined. For all aneurysm neck diameters, ranging from 2 mm to 6 mm, STB remained stable for 3 min at  $10 \text{ mL s}^{-1}$  pulsatile flow; however, at a flow rate of  $15 \text{ mL s}^{-1}$ , all aneurysm models visibly lost a portion of their STB content within the first 3 min—mostly occurring within the first 30 s. Using the same process, STB stability was assessed within the aneurysm models under up to  $25 \text{ mL s}^{-1}$  constant fluid flow (the maximum that the pump could generate), and STB remained visibly stable in all aneurysm models for 3 min.

The proportion of STB remaining in the aneurysm models after 24 h exposure to fluid flow was quantified. Figure 3E presents the percentage of STB mass remaining in the models with varying neck widths under pulsatile flow. STB was fully recovered from the aneurysm models after exposure to  $10 \text{ mL s}^{-1}$  pulsatile flow; however,  $\sim 10\text{--}20\%$  of STB was lost under  $15 \text{ mL s}^{-1}$  pulsatile flow. As evident in Figure 3E, there is no significant correlation between STB loss and neck size for both pulsatile flow rates. Similar to the 3-min observation experiments, either no STB was lost (under  $10 \text{ mL s}^{-1}$  pulsatile flow) or STB loss occurred within the first 30 s (under  $15 \text{ mL s}^{-1}$  pulsatile flow), with no further changes visible over the next 24 h. Comparing the average STB percent remaining for all neck widths, there was no significant difference in recovery between zero (no) flow,  $15 \text{ mL s}^{-1}$  constant flow, and  $10 \text{ mL s}^{-1}$  pulsatile flow, but a significantly lower STB percent remained in the models for  $15 \text{ mL s}^{-1}$  pulsatile flow, as shown in Figure 3F. These findings demonstrate that if STB is initially stable, its resilience does not diminish over the course of 24 h under substantial flow rates. As a comparison, the human femoral artery has an average flow rate of  $5.9 \pm 0.3 \text{ mL s}^{-1}$ .<sup>33</sup>

To test if the STB stability within the *in vitro* aneurysm models would be affected differently by a fluid with a viscosity similar to blood (rather than DPBS), we performed 3-min observational experiments with BMF, which had a viscosity of  $4.1 \pm 0.1 \text{ mPa s}$ . Matching prior experiments performed using DPBS, STB was visibly stable within the first 3 min at  $10 \text{ mL s}^{-1}$  pulsatile flow and was partially lost within the first 15 s at  $15 \text{ mL s}^{-1}$  pulsatile flow (see Supplementary Figure S1). Recovered STB after 24 h could not be quantified due to the BMF containing glycerol and abundant nylon microparticles diffused within the STB over the course of 24 h, adding mass to the STB. Interestingly, the STB changed color from white to red in 24 h, highlighting the penetration of dyed BMF into the STB matrix over time without any visible structural change to the STB (Figure S1). This hints at the potential permissibility of STB to blood penetration and remodeling *in vivo* after aneurysm occlusion and hemostasis, though this needs to be validated in future studies.

### 3.3. Computational fluid dynamics modeling

To better understand the observation that aneurysm neck width did not influence the stability of STB, the shear stress exerted to STB under various flow rates was quantified via 3D finite element flow simulations using CFD, a method that has been validated in experimental *in vitro* aneurysm models.<sup>34,35</sup> The *in vitro* system was modeled according to its dimensions, shown in Figure 4A, with the blood vessel capped at the top of the neck, reflecting the aneurysm occlusion by STB. Flow streamlines for  $15 \text{ mL s}^{-1}$  pulsatile flow, shown in Figure 4B, demonstrate less fluid flow into the neck for the 2 mm aneurysm neck compared with the 6 mm one (Figure 4C). In estimating shear stress at the STB-fluid interface, as shown for  $15 \text{ mL s}^{-1}$  pulsatile flow for the 2 mm neck and 6 mm neck in Figures 4D and 4E, respectively, numerous cases were found in which STB was stable at high shear stress, yet unstable at much lower values of shear stress, depending on the flow pattern and aneurysm neck width. For example, as shown in Figure 4F, the maximum shear stress of 0.98 Pa was exerted on the STB at the STB-fluid interface for the 6 mm neck diameter model under  $15 \text{ mL s}^{-1}$  constant flow. Under this condition, the material was completely stable in the *in vitro* models for 24 h. Conversely, the maximum shear stress estimated from the computer

modeling for the 2 mm neck diameter model under  $15 \text{ mL s}^{-1}$  pulsatile flow was  $10 \times 10^{-3}$  Pa (Figure 4F), yet the material was lost at this condition. These results demonstrate that although neck diameter is a key factor in regulating shear stress at the STB-fluid interface, the magnitude of shear stress is not correlated to the STB loss. In addition, the shear stress tolerated by STB for the 6 mm neck diameter model under  $25 \text{ mL s}^{-1}$  constant flow was 1.89 Pa.

### 3.4. Pressure assessment within in vitro system

Since the magnitude of shear stress failed to explain STB loss in the *in vitro* models, we investigated the effect of pressure change on the STB loss, as shown in Figure 5. Upon recording pressure change profiles for  $10 \text{ mL s}^{-1}$  and  $15 \text{ mL s}^{-1}$  pulsatile flows, we found supraphysiologic pressure ranges and rates of pressure change. In contrast to human blood pressure profiles, which is normally in the range of  $\sim 112$  to  $117.3 \text{ kPa}$  (80 to 120 mmHg) and has a maximum rate of negative pressure change  $-50.3 \pm 3.2 \text{ kPa s}^{-1}$ ,<sup>36</sup>  $10 \text{ mL s}^{-1}$  pulsatile flow was found to have a pressure range of  $\sim 95$  to  $107 \text{ kPa}$  (Figure 5A) and a maximum rate of negative pressure change of  $\sim -107.3 \pm 2.3 \text{ kPa s}^{-1}$ , and  $15 \text{ mL s}^{-1}$  pulsatile flow had a pressure range of  $\sim 92$  to  $111 \text{ kPa}$  (Figure 5B) and a maximum rate of negative pressure change of  $\sim \pm 9.5 \text{ kPa s}^{-1}$ . While the pressure changes under  $10 \text{ mL s}^{-1}$  pulsatile flow were tolerated by the STB for 24 h (Figure 5C), pressure changes under  $15 \text{ mL s}^{-1}$  pulsatile flow were sufficient to cause STB loss within the first 30 s, as shown in Figure 5D. This was followed by STB stability for the remainder of the 24 h after the initial material loss.

### 3.5. In vitro flow experiments with a neck-less aneurysm model

To demonstrate that shear stress is also an important determinant of material stability in addition to pressure changes, we exposed STB to higher shear stress by testing the material in an aneurysm model without a neck. We used the same dimensions as the 6 mm necked aneurysm models, except the aneurysm sac was a hemisphere filled with STB in continuity with the parent vessel rather than a sphere attached to a neck (Figure S2). When exposed to  $15 \text{ mL s}^{-1}$  pulsatile flow for 24 h, 100% of STB was consistently lost, in contrast to the small percentage of material lost under the same flow pattern when the aneurysm neck was present. By independently increasing shear stress on the STB without changing other experimental parameters, we show that additional STB loss can occur with increasing shear stress. Though material failure caused by high shear stress was our initial hypothesis, it was most surprising to find that supraphysiologic pressure changes can cause STB loss even in settings of low shear stress.

### 3.6. Compliance assessment of models

The role of rapid negative pressure change as a cause of material loss or failed aneurysm embolization has not been highlighted previously in the literature, in contrast to the flow parameters, such as shear stress.<sup>37–39</sup> The negative pressure change observed in our study represent an unanticipated limitation of the *in vitro* models that precluded us from being able to assess the stability of STB under entirely physiologic conditions. The low compliance of the PDMS models combined with a pump that delivers a set volume per pump cycle resulted in an unrealistically large pressure ranges, causing STB to initially escape through the

aneurysm neck during the negative pressure phase, as shown in Figure 5D and Supplemental Video 2. To estimate the total compliance of our model system, we considered the ratio of stroke volume to pulse pressure (systolic minus diastolic pressure) as an estimate of total arterial compliance in humans.<sup>40,41</sup> With a stroke volume of 8.33 mL for the 10 mL s<sup>-1</sup> pulsatile flow condition and a stroke volume of 12.5 mL for the 15 mL s<sup>-1</sup> pulsatile flow condition, and the pulse pressures determined from pressure recordings in Figure 5 A-B, total compliance of our model system was estimated around 0.68 mL kPa<sup>-1</sup> (0.09 mL mmHg<sup>-1</sup>), significantly lower than the 10.73 mL kPa<sup>-1</sup> (1.43 mL mmHg<sup>-1</sup>) average total arterial compliance in humans.<sup>40</sup> To achieve a more physiologic pulse pressure of 5.3 kPa (40 mmHg), our compliance in our system would need to be increased about 2.3 times for the 10 mL s<sup>-1</sup> pulsatile flow condition and about 3.5 times for the 15 mL s<sup>-1</sup> pulsatile flow condition—requiring an entirely different aneurysm model fabrication process.

The low compliance of the present aneurysm models is also evident by estimating the normalized vessel compliance per unit length, which can be calculated using vessel radius, vessel wall thickness, and the modulus of elasticity for PDMS.<sup>42</sup> Considering similar PDMS mixing ratios, curing temperatures, and curing times, the Young's modulus of our PDMS models is around 1.49 MPa.<sup>43</sup> Using this modulus of elasticity and aforementioned vessel dimensions, the normalized compliance of the PDMS models per unit length is  $4.03 \times 10^{-7}$  Pa<sup>-1</sup>—only about 1.3% of the normalized compliance of the human aorta ( $3.13 \times 10^{-5}$  Pa<sup>-1</sup>).<sup>42</sup> Though this value does not represent the entire system compliance, which is also affected by connector tubing and pump inflow reservoir variables, it highlights the importance of increased vessel compliance for future aneurysm models.

With previous *in vitro* aneurysm testing systems not considering system compliance,<sup>44,45</sup> including those testing endovascular treatments such as coils and stents,<sup>46,47</sup> the critical role of compliance in our STB testing system was an unexpected and important finding. Future *in vitro* aneurysm testing systems, particularly those for testing non-metallic material occlusion of aneurysms, must consider system compliance for generating realistic pressure ranges; methods for increasing compliance of synthetic vessels without changing model dimensions include decreasing the material's modulus of elasticity and decreasing vessel wall thickness.<sup>42,48</sup> While simple in theory, producing synthetic blood vessels with a compliance matching native ones has proven to be challenging from an engineering standpoint.<sup>48,49</sup> Various methods have attempted to produce compliant, thin synthetic blood vessels, including molding,<sup>42,50</sup> brush-spin-coating,<sup>51</sup> and dip-coating,<sup>52</sup> usually using silicone or latex.<sup>48</sup> Such models may be useful for future *in vitro* aneurysm testing applications, but come with their own limitations, including variable wall thickness and compliance<sup>50</sup> and poor compliance congruity over a range of physiologic pressures.<sup>48</sup> Though reassured by the STB's tolerance of suprphysiologic pressure ranges under 10 mL s<sup>-1</sup> pulsatile flow for 24 h, we note that limitations in our testing system and other *in vitro* systems make further testing necessary, particularly in animal aneurysm models.<sup>53</sup>

#### 4. Conclusions

We show that catheter-directed STB injection is a minimally invasive method capable of occluding saccular aneurysms/pseudoaneurysms *in vitro*. The biomaterial can be easily

prepared, injected by hand, and completely fill aneurysm spaces. It is effective in holding its gel form after injection and remaining in place within *in vitro* aneurysm models exposed to constant fluid flow rates up to  $15 \text{ mL s}^{-1}$  for 24 h. The material also withstood a pulsatile flow rate of  $10 \text{ mL s}^{-1}$  for 24 h, mimicking flow through the human femoral artery. The STB did not disintegrate over this period to any degree that could be detected by both visual inspection and mass quantification. STB was also able to withstand at least  $1.89 \text{ Pa}$  of wall shear stress, as estimated by computational fluid dynamics, without visible mass loss. We found that our *in vitro* system was limited by supraphysiologic pressure changes caused by PDMS aneurysm models with low compliance, rather than shear stress, resulting in STB failure. Though this is a critical consideration for the design of future *in vitro* testing systems, we were encouraged by the STB resistance to negative pressure changes that were wider ranging and more rapidly changing than those in the human aorta. The ultimate applicability of STB for the occlusion of human aneurysms will depend on further testing in more realistic *in vitro* models and particularly in animal aneurysm models.

## Supplementary Material

Refer to Web version on PubMed Central for supplementary material.

## Acknowledgements

A. K. acknowledges the financial support from the National Institutes of Health (NIH) through HL140951. A. S. would like to acknowledge the financial support from the Canadian Institutes of Health Research (CIHR) through a post-doctoral fellowship as well as the startup fund from The Pennsylvania State University.

## Abbreviations:

|              |                                      |
|--------------|--------------------------------------|
| <b>VAA</b>   | visceral artery aneurysms            |
| <b>VAPA</b>  | visceral artery pseudoaneurysms      |
| <b>STB</b>   | shear-thinning biomaterial           |
| <b>DMSO</b>  | dimethyl sulfoxide                   |
| <b>ABS</b>   | acrylonitrile butadiene styrene      |
| <b>PDMS</b>  | polydimethylsiloxane                 |
| <b>DPBS</b>  | Dulbecco's phosphate buffered saline |
| <b>BMF</b>   | blood mimicking fluid                |
| <b>CFD</b>   | computational fluid dynamics         |
| <b>ANOVA</b> | analysis of variance                 |
| <b>CAD</b>   | computer-aided design                |

## References

1. Hosn MA, Xu J, Sharafuddin M, Corson JD. Visceral Artery Aneurysms: Decision Making and Treatment Options in the New Era of Minimally Invasive and Endovascular Surgery. *Int J Angiol* 2019;28(1):11–16. doi:10.1055/s-0038-1676958 [PubMed: 30880885]
2. Tipaldi MA, Krokidis M, Orgera G, et al. Endovascular management of giant visceral artery aneurysms. *Sci Rep* 2021;11(1):1–6. doi:10.1038/s41598-020-80150-2 [PubMed: 33414495]
3. Loffroy R, Favelier S, Pottecher P, et al. Endovascular management of visceral artery aneurysms: When to watch, when to intervene? *World J Radiol* 2015;7(7):143. doi:10.4329/wjr.v7.i7.143 [PubMed: 26217453]
4. Chiaradia M, Novelli L, Deux J-F, et al. Ruptured visceral artery aneurysms. *Diagn Interv Imaging* 2015;96(7–8):797–806. doi:10.1016/j.diii.2015.03.012 [PubMed: 26054246]
5. Sachdev U, Baril DT, Ellozy SH, et al. Management of aneurysms involving branches of the celiac and superior mesenteric arteries: A comparison of surgical and endovascular therapy. *J Vasc Surg* 2006;44(4):718–724. doi:10.1016/j.jvs.2006.06.027 [PubMed: 17011997]
6. Ruhnke H, Kröncke TJ. Visceral Artery Aneurysms and Pseudoaneurysms: Retrospective Analysis of Interventional Endovascular Therapy of 43 Aneurysms. *RoFo Fortschritte auf dem Gebiet der Röntgenstrahlen und der Bildgeb Verfahren* 2017:632–639. doi:10.1055/s-0043-107239
7. Madhusudhan KS, Venkatesh HA, Gamanagatti S, Garg P, Srivastava DN. Interventional radiology in the management of visceral artery pseudoaneurysms: A review of techniques and embolic materials. *Korean J Radiol* 2016;17(3):351–363. doi:10.3348/kjr.2016.17.3.351 [PubMed: 27134524]
8. Sadasivan C, Lieber BB. Numerical Investigation of Coil Configurations That Provide Ultrahigh Packing Density of Saccular Aneurysms. *J Med Device* 2009;3(4):1–7. doi:10.1115/1.4000453
9. Bavinski G, Talazoglu V, Killer M, et al. Gross and microscopic histopathological findings in aneurysms of the human brain treated with Guglielmi detachable coils. *J Neurosurg* 1999;91(2):284–293. doi:10.3171/jns.1999.91.2.0284 [PubMed: 10433317]
10. Choi J, Kim YM. A Rare Case of Coil Migration into the Duodenum after Embolization of a Right Colic Artery Pseudoaneurysm. *Clin Endosc* 2021;10–13. doi:10.5946/ce.2020.228
11. Nomura Y, Gotake Y, Okada T, Yamaguchi M, Sugimoto K, Okita Y. Coil Migration to the Duodenum 1 Year Following Embolisation of a Ruptured Giant Common Hepatic Artery Aneurysm. *EJVES Short Reports* 2018;39:33–36. doi:10.1016/j.ejvssr.2018.05.001 [PubMed: 29988858]
12. Fiorella D, Albuquerque FC, McDougall CG. Durability of aneurysm embolization with matrix detachable coils. *Neurosurgery* 2006;58(1):51–58. doi:10.1227/01.NEU.0000194190.45595.9E [PubMed: 16385329]
13. Simon SD, Reig AS, James RF, Reddy P, Mericle RA. Relative cost comparison of embolic materials used for treatment of wide-necked intracranial aneurysms. *J Neurointerv Surg* 2010;2(2):163–167. doi:10.1136/jnis.2009.001719 [PubMed: 21990601]
14. Pitton MB, Dappa E, Jungmann F, et al. Visceral artery aneurysms: Incidence, management, and outcome analysis in a tertiary care center over one decade. *Eur Radiol* 2015;25(7):2004–2014. doi:10.1007/s00330-015-3599-1 [PubMed: 25693662]
15. Gonzalez-Araiza G, Haddad L, Karageorgiou J. Migration of Nonfibered Packing Coils Used to Treat Peripheral Pseudoaneurysms: Report of 3 Cases. *J Vasc Interv Radiol* 2019;30(11):1840–1844.e1. doi:10.1016/j.jvir.2019.06.007 [PubMed: 31587948]
16. Bratby MJ, Lehmann ED, Bottomley J, et al. Endovascular embolization of visceral artery aneurysms with ethylene-vinyl alcohol (Onyx): A case series. *Cardiovasc Intervent Radiol* 2006;29(6):1125–1128. doi:10.1007/s00270-005-0148-3 [PubMed: 16625409]
17. Qureshi AI, Mian N, Siddiqi H, et al. Occurrence and Management Strategies for Catheter Entrapment with Onyx Liquid Embolization. *J Vasc Interv Neurol* 2015;8(3):37–41.
18. Chaloupka JC, Huddle DC, Alderman J, Fink S, Hammond R, Vinters HV. A reexamination of the angiotoxicity of superselective injection of DMSO in the swine rete embolization model. *Am J Neuroradiol* 1999;20(3):401–410. [PubMed: 10219404]

19. Gaharwar AK, Avery RK, Assmann A, et al. Shear-Thinning Nanocomposite Hydrogels for the Treatment of Hemorrhage. *ACS Nano* 2014;8(10):9833–9842. doi:10.1021/nn503719n [PubMed: 25221894]
20. Avery RK, Albadawi H, Akbari M, et al. An injectable shear-thinning biomaterial for endovascular embolization. *Sci Transl Med* 2016;8(365). doi:10.1126/scitranslmed.aah5533
21. Zhou G, Zhu Y, Yin Y, Su M, Li M. Association of wall shear stress with intracranial aneurysm rupture: Systematic review and meta-analysis. *Sci Rep* 2017;7(1):1–8. doi:10.1038/s41598-017-05886-w [PubMed: 28127051]
22. Graziano F, Russo VM, Wang W, Khismatullin D, Ulm AJ. 3D Computational Fluid Dynamics of a Treated Vertebrobasilar Giant Aneurysm: A Multistage Analysis. *Am J Neuroradiol* 2013;34(7):1387–1394. doi:10.3174/ajnr.a3373 [PubMed: 23306008]
23. Shibata E, Takao H, Amemiya S, Ohtomo K. 3D-printed visceral aneurysm models based on ct data for simulations of endovascular embolization: Evaluation of size and shape accuracy. *Am J Roentgenol* 2017;209(2):243–247. doi:10.2214/AJR.16.17694 [PubMed: 28731812]
24. Da Silveira LA, Silveira FBC, Fazan VPS. Arterial diameter of the celiac trunk and its branches. Anatomical study. *Acta Cir Bras* 2009;24(1):043–047. doi:10.1590/S0102-86502009000100009
25. Xu J, Wu Z, Yu Y, et al. Combined effects of flow diverting strategies and parent artery curvature on aneurysmal hemodynamics: A CFD study. *PLoS One* 2015;10(9):1–13. doi:10.1371/journal.pone.0138648
26. Sheikh MAA, Shuib AS, Mohyi MHH. A review of hemodynamic parameters in cerebral aneurysm. *Interdiscip Neurosurg Adv Tech Case Manag* 2020;22 (November 2019):100716. doi:10.1016/j.inat.2020.100716
27. Tang AYS, Chung WC, Liu ETY, et al. Computational Fluid Dynamics Study of Bifurcation Aneurysms Treated with Pipeline Embolization Device: Side Branch Diameter Study. *J Med Biol Eng* 2015;35(3):293–304. doi:10.1007/s40846-015-0046-3 [PubMed: 26167140]
28. Fennell VS, Kalani MYS, Atwal G, Martirosyan NL, Spetzler RF. Biology of Saccular Cerebral Aneurysms: A Review of Current Understanding and Future Directions. *Front Surg* 2016;3(July):1–8. doi:10.3389/fsurg.2016.00043 [PubMed: 26835458]
29. Kimura M, Hoshina K, Kobayashi M, Yamamoto S, Ohshima M, Watanabe T. Morphological analysis using geometric parameters for splenic aneurysms. *Asian Cardiovasc Thorac Ann* 2018;26(2):133–138. doi:10.1177/0218492318757040 [PubMed: 29363319]
30. Wilcox DC. *Turbulence Modeling for CFD* 2nd ed. La Canada, CA: DCW industries; 1998.
31. Sheikh A, Afewerki S, Oklu R, Gaharwar AK, Khademhosseini A. Effect of ionic strength on shear-thinning nanoclay-polymer composite hydrogels. *Biomater Sci* 2018;6(8):2073–2083. doi:10.1039/c8bm00469b [PubMed: 29944151]
32. Saad Nael E. A., Saad Wael E. A., Davies Mark G., Waldman David L., Fultz DJR Patrick J.. PERIPHERAL VASCULAR DIAGNOSIS AND INTERVENTIONS Pseudoaneurysms and the Role of Minimally Invasive Techniques in Their Management 2005:173–190.
33. Maroto A, Gines P, Arroyo V, et al. Brachial and femoral artery blood flow in cirrhosis: relationship to kidney dysfunction. *Hepatology* 1993;17(5):788–793. [PubMed: 8491446]
34. Tsang ACO, Lai SSM, Chung WC, et al. Blood flow in intracranial aneurysms treated with pipeline embolization devices: Computational simulation and verification with Doppler ultrasonography on phantom models. *Ultrasonography* 2015;34(2):98–108. doi:10.14366/usg.14063 [PubMed: 25754367]
35. Shi C, Kojima M, Anzai H, et al. In vitro strain measurements in cerebral aneurysm models for cyber-physical diagnosis. *Int J Med Robot* 2013;9(2):213–222. doi:10.1002/rcs.1487 [PubMed: 23483681]
36. Brinton TJ, Cotter B, Kailasam MT, et al. Development and validation of a noninvasive method to determine arterial pressure and vascular compliance. *Am J Cardiol* 1997;80(3):323–330. doi:10.1016/S0002-9149(97)00353-6 [PubMed: 9264426]
37. Luo B, Yang X, Wang S, et al. High shear stress and flow velocity in partially occluded aneurysms prone to recanalization. *Stroke* 2011;42(3):745–753. doi:10.1161/STROKEAHA.110.593517 [PubMed: 21233477]

38. Irie K, Kojima M, Negoro M, et al. Computational fluid dynamic analysis following recurrence of cerebral aneurysm after coil embolization. *Asian J Neurosurg* 2012;7(3):109. doi:10.4103/1793-5482.103706 [PubMed: 23293665]
39. Zhang Q, Jing L, Liu J, et al. Predisposing factors for recanalization of cerebral aneurysms after endovascular embolization: A multivariate study. *J Neurointerv Surg* 2018;10(3):252–257. doi:10.1136/neurintsurg-2017-013041 [PubMed: 28377443]
40. Chemla D, Hébert JL, Coirault C, et al. Total arterial compliance estimated by stroke volume-to-aortic pulse pressure ratio in humans. *Am J Physiol - Hear Circ Physiol* 1998;274(2 43–2). doi:10.1152/ajpheart.1998.274.2.h500
41. Homan TD, Bordes S, Cichowski E. Physiology, Pulse Pressure. *StatPearls* 2021;30(2):29494015. <https://www.ncbi.nlm.nih.gov/books/NBK482408/>.
42. Yazdi SG, Huetter L, Docherty PD, et al. A novel fabrication method for compliant silicone phantoms of arterial geometry for use in particle image velocimetry of haemodynamics. *Appl Sci* 2019;9(18). doi:10.3390/app9183811
43. Hocheng H, Chen CM, Chou YC, Lin CH. Study of novel electrical routing and integrated packaging on bio-compatible flexible substrates. *Microsyst Technol* 2010;16(3):423–430. doi:10.1007/s00542-009-0930-2
44. Medero Rafael, PhD1, 2, Ruedinger Katrina, MS3, 4, Rutkowski David, PhD1, 2, Johnson Kevin, PhD5, Roldán-Alzate Alejandro, PhD1, 2 3 1Department. In Vitro Assessment of Flow Variability in an Intracranial Aneurysm Model using 4D Flow MRI and Tomographic PIV Rafael. *Physiol Behav* 2017;176(12):139–148. doi:10.1007/s10439-020-02543-8.In [PubMed: 28363838]
45. Levitt MR, Mandrycky C, Abel A, et al. Genetic correlates of wall shear stress in a patient-specific 3D-printed cerebral aneurysm model. *J Neurointerv Surg* 2019;11(10):999–1003. doi:10.1136/neurintsurg-2018-014669 [PubMed: 30979845]
46. Chivukula VK, Levitt MR, Clark A, et al. Reconstructing patient-specific cerebral aneurysm vasculature for in vitro investigations and treatment efficacy assessments. *J Clin Neurosci* 2020;153–159. doi:10.1016/j.jocn.2018.10.103.Reconstructing
47. Villadolid C, Puccini B, Dennis B, Gunnin T, Hedigan C, Cardinal KO. Custom tissue engineered aneurysm models with varying neck size and height for early stage in vitro testing of flow diverters. *J Mater Sci Mater Med* 2020;31(3). doi:10.1007/s10856-020-06372-y
48. Byrne O, Coulter F, Roche ET, O’Cearbhaill ED. In silico design of additively manufacturable composite synthetic vascular conduits and grafts with tuneable compliance. *Biomater Sci* 2021;9(12):4343–4355. doi:10.1039/d0bm02169e [PubMed: 33724267]
49. Lucereau B, Koffhi F, Lejay A, et al. Compliance of Textile Vascular Prostheses Is a Fleeting Reality. *Eur J Vasc Endovasc Surg* 2020;60(5):773–779. doi:10.1016/j.ejvs.2020.07.016 [PubMed: 32792290]
50. Marconi S, Lanzarone E, van Bogerijen GHW, et al. A compliant aortic model for in vitro simulations: Design and manufacturing process. *Med Eng Phys* 2018;59:21–29. doi:10.1016/j.medengphy.2018.04.022 [PubMed: 30077485]
51. Chi QZ, Mu LZ, He Y, Luan Y, Jing YC. A Brush–Spin–Coating Method for Fabricating In Vitro Patient-Specific Vascular Models by Coupling 3D-Printing. *Cardiovasc Eng Technol* 2021;12(2):200–214. doi:10.1007/s13239-020-00504-9 [PubMed: 33263929]
52. Behr JM, Irvine SA, Thwin CS, et al. Matching Static and Dynamic Compliance of Small-Diameter Arteries, with Poly(lactide-co-caprolactone) Copolymers: In Vitro and In Vivo Studies. *Macromol Biosci* 2020;20(3):1–15. doi:10.1002/mabi.201900234
53. Marbacher S, Strange F, Frösén J, Fandino J. Preclinical extracranial aneurysm models for the study and treatment of brain aneurysms: A systematic review. *J Cereb Blood Flow Metab* 2020;40(5):922–938. doi:10.1177/0271678X20908363 [PubMed: 32126875]

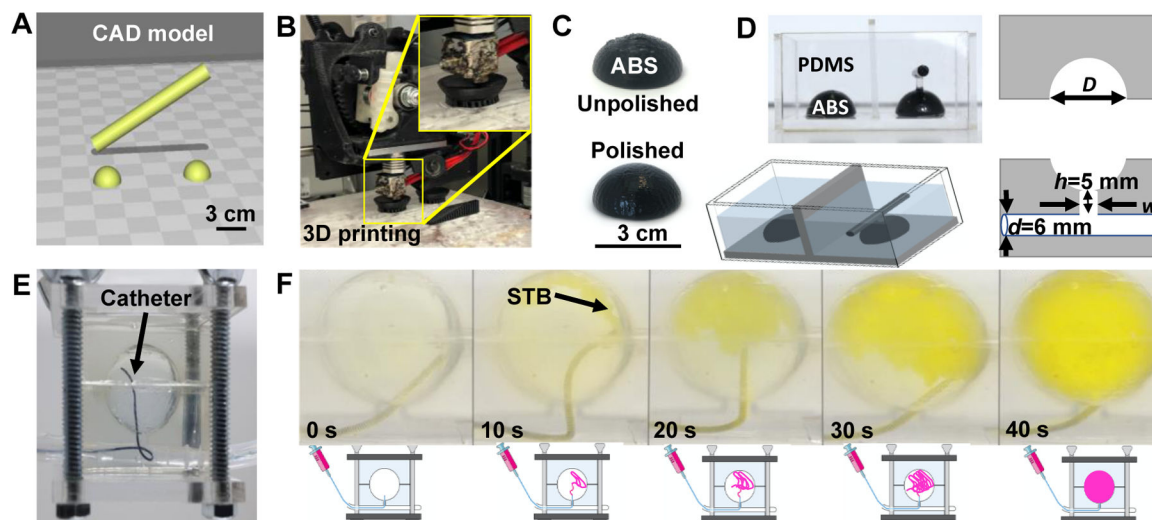


**Fig. 1. Fabrication of *in vitro* aneurysm models and filling them with STB.**

(A) CAD-based fabrication of aneurysm model components, including a parent artery and the saccular aneurysm pieces. (B) 3D-printing of aneurysm model components using ABS. (C) Polishing the surface of 3D printed ABS pieces to render the surfaces smooth. (D) Formation of negative PDMS mold using the 3D printed ABS pieces, and the removal of ABS yielding aneurysm models with the following dimensions: blood vessel diameter,  $d$ : 6 mm, neck height,  $h$ : 5 mm, neck diameter (width),  $w$ : variable (2, 3, 4, 5, or 6 mm), and aneurysm sac diameter,  $D$ : variable (1 cm or 3 cm). (E) Navigation of a catheter into a 3 cm diameter aneurysm model. (F) Time course of STB filling of the 3 cm aneurysm model using a microcatheter under pulsatile flow in less than 1 min. The STB is stained with commercial yellow food dye.

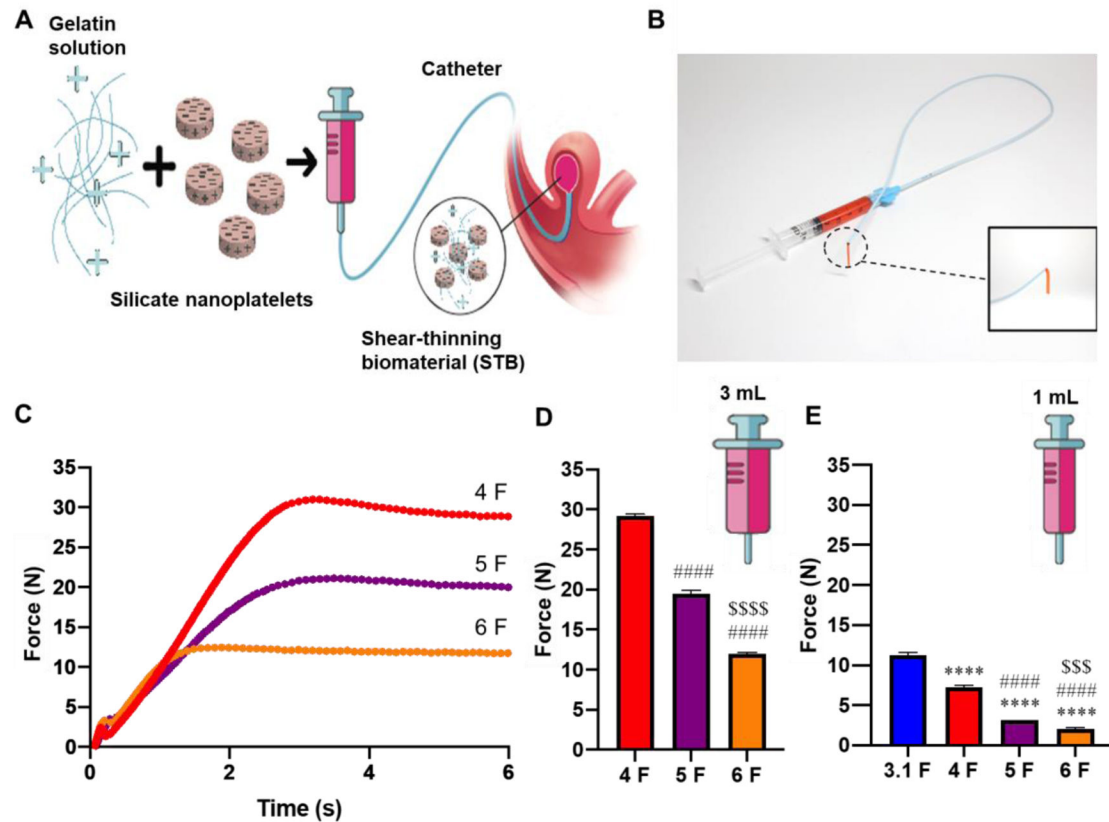


**Fig. 2. Formulation and properties of shear-thinning biomaterial (STB).**

(A) Gelatin and LAPONITE® XLG-XR (silicate nanoplatelets) are mixed to form STB, which is injected into an aneurysm using a catheter. (B) Picture of colored STB loaded into a syringe and injected via a catheter. (C) Injection force versus injection time and (D) injection force plateaus for STB injected through catheters connected to a 3 mL syringe at a syringe depression rate of  $33.96 \text{ mm min}^{-1}$ . (E) Injection force plateaus for STB injected through catheters connected to a 1 mL syringe at the same rate of syringe depression as in panel D. One-way ANOVA with multiple comparisons (Tukey post-test) were performed: \* indicates comparison with 3.1 F; # shows comparison with 4 F; and \$ is for the comparison with 5 F (\*\*\*, ###, or \$\$\$ indicate  $p < 0.001$ ; \*\*\*\*, #####, or \$\$\$\$ show  $p < 0.0001$ ).

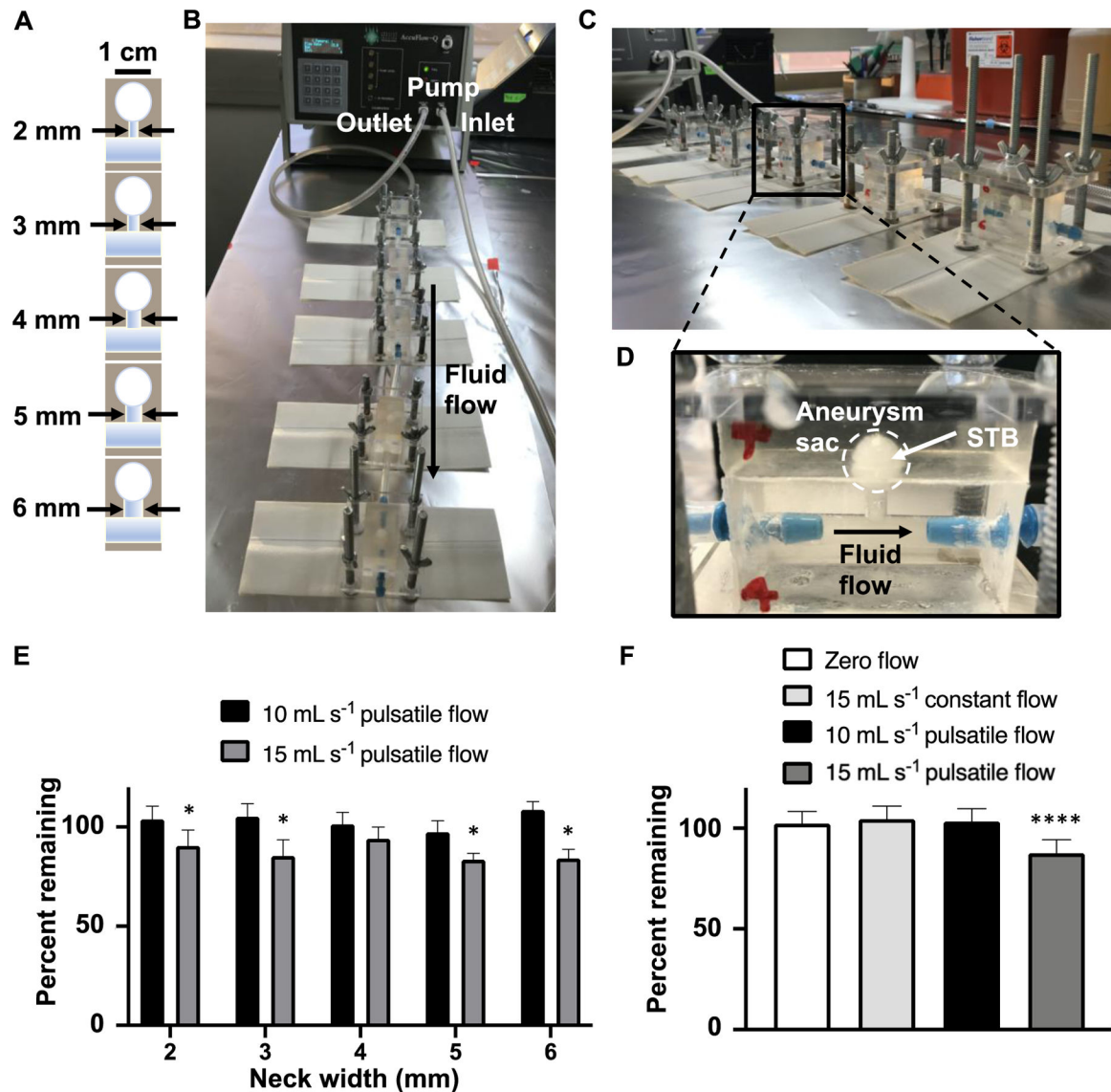


**Fig. 3. Stability of STB in aneurysm models over 24 h.**

(A) Schematic of 1 cm aneurysm models used in 24-h flow experiments, with the neck width ranging from 2 to 6 mm. (B and C) Experimental setup showing the AccuFlow-Q Physiological Flow System connected to aneurysm models in series. (D) Close-up image of a 1 cm aneurysm model with a 4 mm neck width, showing the sac filled with STB. (E) Comparison of the percent STB recovered from models with neck widths ranging from 2 to 6 mm exposed to 10 mL s<sup>-1</sup> and 15 mL s<sup>-1</sup> pulsatile flows after 24 h, showing significant differences (One-way ANOVA with multiple comparisons (Fisher's post-test); \*  $p < 0.05$ ) for all aneurysm neck sizes except the 4 mm neck. (F) STB percent remaining after 24 h from all neck sizes for zero flow, 15 mL s<sup>-1</sup> constant flow, 10 mL s<sup>-1</sup> pulsatile flow, and 15 mL s<sup>-1</sup> pulsatile flow, showing significant differences (One-way ANOVA with multiple comparisons (Tukey post-test); \*\*\*\*  $p < 0.0001$ ) for 15 mL s<sup>-1</sup> pulsatile flow compared with all other flow patterns.

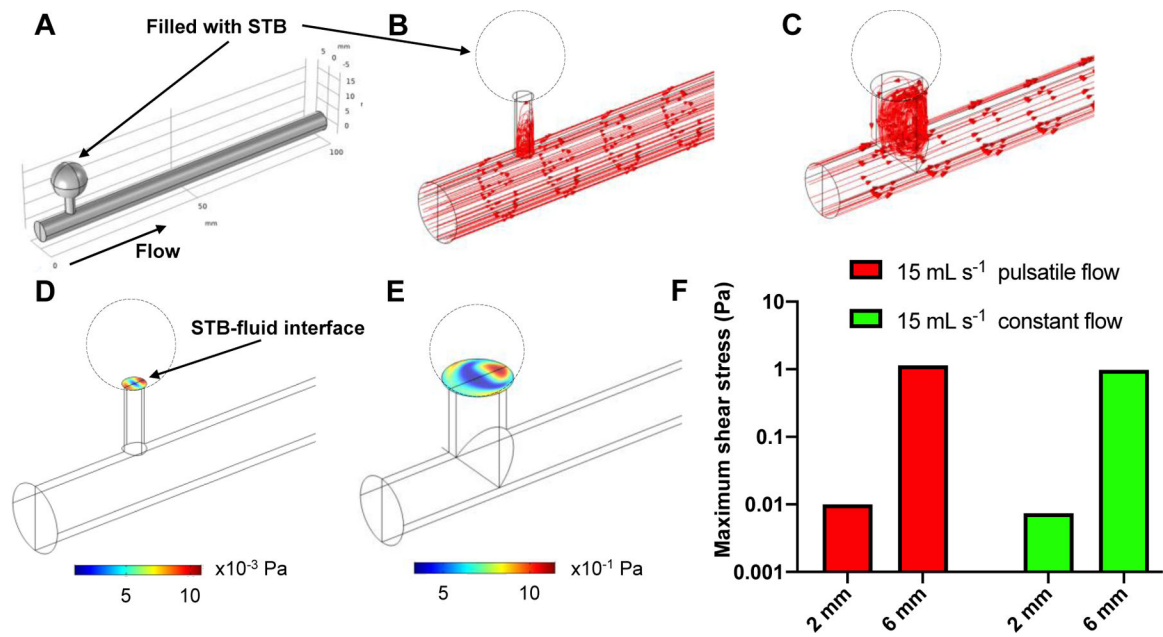


**Fig. 4. CFD simulation of fluid flow in aneurysm models.**

(A) Simulation computational domain, comprising a finite length 3D conduit that is 100 mm long with an inner diameter of 6 mm, connected to an aneurysm sac through a 5 mm long cylindrical neck of a diameter varying from 2 mm to 6 mm. For the simulation, the neck was capped at the STB-fluid interface to reflect the *in vitro* experiments in which STB filled the aneurysm sac. (B and C) Flow streamlines determined by CFD for 15 mL s<sup>-1</sup> pulsatile flow, demonstrating more fluid flow into the aneurysm neck for the 6 mm neck compared with the 2 mm neck. (D) Shear stress as determined from CFD modeling at the STB-fluid interface for the 2 mm neck aneurysm model experiencing 15 mL s<sup>-1</sup> pulsatile flow. (E) Shear stress as determined from CFD modeling at the STB-fluid interface for the 6 mm neck aneurysm model experiencing 15 mL s<sup>-1</sup> pulsatile flow. (F) Magnitude of maximum shear stress at the STB-fluid interface for the 2 mm and 6 mm neck-size aneurysm models under 15 mL s<sup>-1</sup> pulsatile flow and 15 mL s<sup>-1</sup> constant flow, demonstrating a discordance between maximal shear stress and material stability (STB was stable for 24 h under 15 mL s<sup>-1</sup> constant flow regardless of aneurysm neck size, whereas it was lost within 24 h under 15 mL s<sup>-1</sup> pulsatile flow regardless of aneurysm neck size).

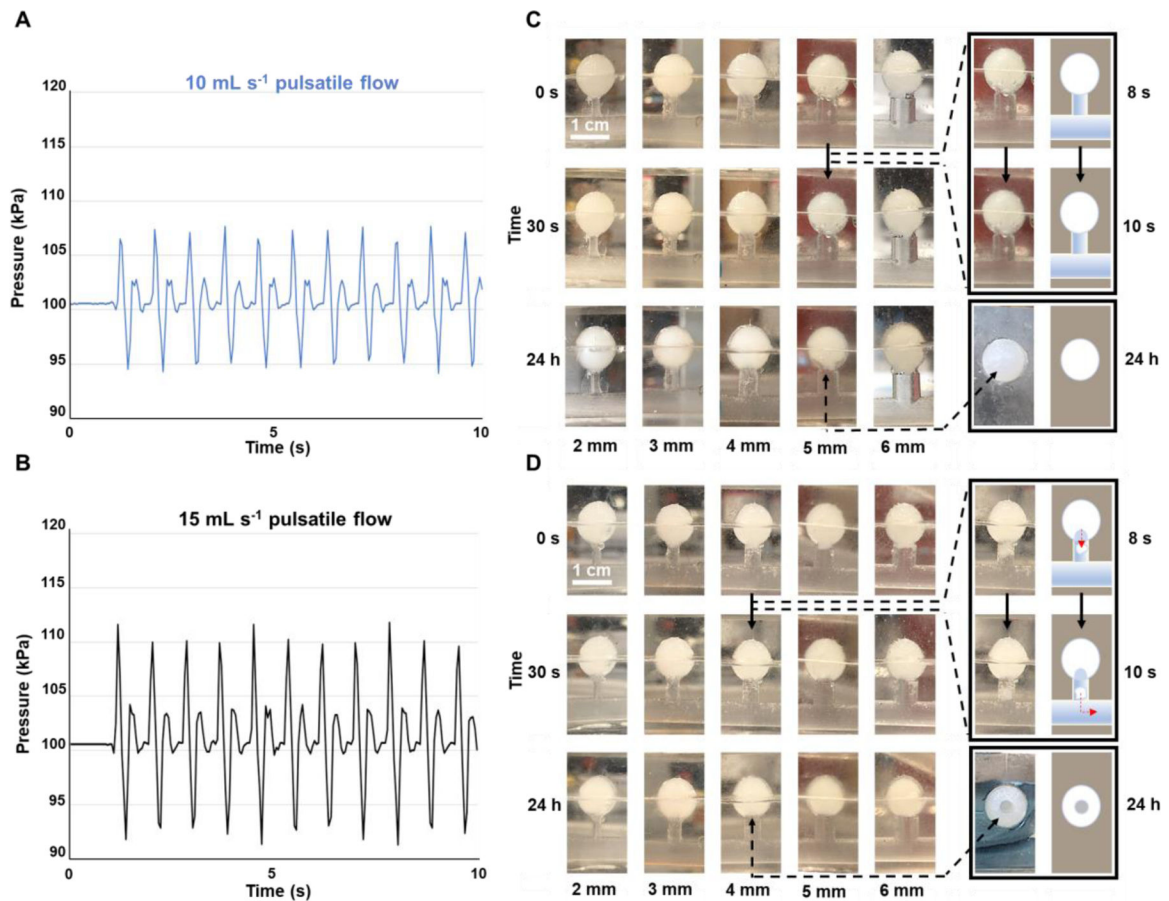


**Fig. 5. Supraphysiologic pressure changes resulting in STB loss.**

Pressure versus time for 10 mL s<sup>-1</sup> and **(B)** 15 mL s<sup>-1</sup> pulsatile flow. **(C)** Images of 1 cm aneurysm models ranging from 2 mm to 6 mm neck widths under 10 mL s<sup>-1</sup> pulsatile flow at varying time points, demonstrating the stability of STB for 24 h. **(D)** Images of 1 cm aneurysm models ranging from 2 mm to 6 mm neck widths under 15 mL s<sup>-1</sup> pulsatile flow at varying time points, showing STB loss within the first 30 s, followed by no additional material loss for the remainder of the 24 h.